www.ietdl.org

Published in IET Microwaves, Antennas & Propagation
Received on 27th April 2013
Revised on 25th June 2013
Accepted on 3rd July 2013
doi: 10.1049/iet-map.2013.0218

ISSN 1751-8725

Mutual coupling compensation for a practical VHF/UHF Yagi-Uda antenna array

Naser Parhizgar[1], Abbas Alighanbari[2], Mohammad-Ali Masnadi-Shirazi[2], Abbas Sheikhi[2]

[1]*Department of Electrical Engineering, Science and Research Branch, Islamic Azad University, Fars, Iran*
[2]*Faculty and Computer Engineering, Department of Communications and Electronics Engineering, Shiraz University, Shiraz, Iran*
E-mail: parhizgar@fsriau.ac.ir

Abstract: The performance of an antenna array is considerably affected by mutual coupling effects between antenna elements. When a large number of antenna elements are located close to each other, mutual coupling becomes more significant. In this study, by using a new mutual impedance matrix, a decoupling methodology for compensating mutual coupling effects in a practical very high frequency (VHF)/ultra high frequency (UHF) Yagi-Uda antenna array is introduced. No previous publications have studied VHF/UHF Yagi-Uda antenna arrays in this context. In the proposed scheme, extreme care has been taken to account for both self- and mutual impedance related to mutual coupling effects. Experimental and simulation results show that using the proposed method, a perfect decoupling is achieved. The application of high-resolution direction of arrival (DOA) estimation algorithms in decoupled experimental data leads to excellent performance of DOA estimation, in terms of accuracy and resolution. In addition, it is concluded (from experimental and simulation results) that mutual coupling effects between array elements as well as the root-mean-square error of estimated parameters depend on the direction of arrival. It is also deduced that in the presence of mutual coupling, estimation of signal parameter via rotation invariance techniques algorithm performs better than other subspace-based algorithms.

1 Introduction

Antenna arrays in receiving mode are widely used to scan space and provide spatial information about the existence of signal sources. Direction of arrival (DOA) estimation using sensor arrays is an important problem in many applications and is the base of most adaptive array processing algorithms. DOA of the signals which impinge the array should be estimated before applying the required adaptive techniques. A wide range of papers have been published in the context of subspace-based methods such as multiple signal classification (MUSIC), root-MUSIC algorithm and the estimation of signal parameter via rotation invariance techniques (ESPRIT). The methods are capable of separating closely spaced sources and provide high-resolution DOA estimation of the signals [1–5]. Practically, these algorithms may often be seriously affected by mutual coupling among array elements. The algorithms mentioned above are classified as model-based parameter estimation (MBPE) algorithms, they assume no mutual coupling between the array elements [6]. However, when the array is affected by mutual coupling effects, the steering vector does not satisfy the model. In ideal situations, the steering vector is supposed to be known depending heavily on geometry of the array and signal position. This is not an exact supposition, since the steering vector in practical arrays can be distorted by mutual coupling, array gain/phase ambiguities and sensor location perturbation [7]. Mutual coupling among the array elements can significantly degrade the performance of high-resolution DOA estimation techniques mentioned above and associated signal processing algorithms [6–11]. Hereupon, this undesired effect has attracted the attention of many researchers who work in this context [6, 12–21]. The present study focuses on the methods which use mutual impedance matrices (MIMs) to compensate the mutual coupling effects. Gupta and Ksienski in [8] investigated mutual coupling effects on the performance of adaptive antennas using a MIM technique. Authors in the above reference have modelled the mutual coupling effects of an antenna array as an $(N+1)$-terminal linear time-invariant (LTI) network. The MIM transforms the terminal voltages to the so-called 'open-circuit voltages'. Then, these voltages can be applied to the array signal processing algorithms such as DOA estimation and beamforming.

As shown in [12, 13], the 'open-circuit voltages' are the voltages in the presence of the other open circuited antenna elements. In the above, the effects of mutual coupling have been reduced but not removed. As an alternative, a modified decoupling method has been presented in [13, 14]. A different formulation has been also introduced, through which, 'receiving mutual impedance matrix' (RMIM) is calculated. This scheme was typically represented in [15–17, 19] to compensate the mutual coupling effects with the application to estimate DOA of signals and adaptive nulling of interference signals. Reference [19] has presented

a scheme for calculating the MIM, as follows. For antenna arrays with simple omnidirectional antennas, such as monopoles or dipoles, the current distribution remains unchanged at their resonant frequencies regardless of the azimuth angle of arrival, whereas the elevation angle of an arrival signal is not too far from the plane perpendicular to the axis of the antenna. Therefore mutual impedances between array elements are invariant with respect to the azimuth angle of incoming signals. Taking benefit of this observation, the currents and voltages of antenna terminals, at $N-1$ distinct angles of incoming signal, φ_n, $n=1,2,\ldots, N-1$ can be measured. The data is then used for computing mutual impedance between each pair of elements by simultaneous calculation of $N-1$ mutual impedance of an N-element array [19].

Generally, the mutual impedance between each pair of elements in the receiving antenna array depends on the DOA of the signal. As mentioned before, when antenna elements have an omnidirectional radiation pattern, as in dipole or monopole antennas, the mutual impedance is independent of the DOA of the incident signal [13–15]. However, it is not true for the antenna arrays with directional antennas in the wide sense [18]. Although in the limited sense for arrays with directional antenna elements, such as Yagi-Uda arrays, which is constructed of thin wire elements, the current distribution is fixed as far as the azimuth angle of incidence is not too far from the plane normal to the array, and is almost perpendicular to the axis of the wires (i.e. $70^\circ \le \varphi \le 110^\circ$) [13–15]. Therefore mutual impedances are invariant with respect to this limited azimuth angle of arrival. All the aforementioned literature were about the antenna array with omnidirectional antennas. Recently, Celik *et al.* [22], have experimentally evaluated the performance of a smart antenna system with directional elements. Their effort confirmed the advantage of Yagi-Uda antennas to omnidirectional ones in DOA estimation of impinging signals.

This paper investigates the decoupling methodology for compensating mutual coupling effects in a practical VHF/UHF Yagi-Uda antenna array by using a new MIM model. As pointed out in [20, 21], the scheme of the above-mentioned references is not precise, and some mutual coupling terms have been ignored. In the new method, extreme care has been taken to account for both self-impedance and mutual impedances, relating to mutual coupling effects. As shown in [20, 21] these newly calculated MIM can, more efficiently, eliminate the mutual coupling effects in a ULA with application to DOA estimation and related topics, such as adaptive nulling. In this work, a new MIM for compensating mutual coupling effects in VHF/UHF Yagi-Uda antenna array and decoupling methodology is introduced.

Moreover, the performance of high-resolution DOA estimation algorithms in the presence of mutual coupling for a VHF/UHF antenna array is evaluated. The performance of MUSIC, root-MUSIC and ESPRIT algorithms are evaluated and compared with each other based on four types of input data: The ideal data without mutual coupling effect, the data captured by full-wave electromagnetic method of moment (MOM) algorithm [23, 24] (electromagnetic simulation (EMS) data), the experimental data without decoupling obtained from the VHF/UHF Yagi-Uda array at the antenna array research lab at Shiraz University (AARL-SU), and the experimental data modified by the method proposed at this study. Experimental and simulation results manifest that mutual coupling effects between array elements and mean square error (MSE) of the estimated parameter are functions of the DOA of the incident signal. It is also deduced that, in the presence of mutual coupling, ESPRIT algorithm performs better than other algorithms.

The rest of the paper is organised as follows. In Section 2, to compensate mutual coupling, a method for calculating a modified MIM is introduced. The experimental equipment used for capturing the required data are introduced in Section 3. In Section 4, the mutual coupling compensation capability of the proposed method for a practical four-element VHF/UHF Yagi-Uda antenna array is evaluated experimentally. To evaluate the mutual coupling compensation capability of the proposed scheme, three scenarios are presented. Finally, the conclusions are presented.

2 Modified MIM and method for its calculation

Consider a collinear VHF/UHF Yagi-Uda antenna array which is constructed with P VHF/UHF Yagi-Uda antennas. Each of the Yagi-Uda antennas are made of Q wire elements (here, $P=4$ and $Q=16$). The Yagi-Uda antennas are connected to the terminal load impedance Z_L at their feed points (central segments of the fed wire elements). The antenna array in receiving mode is assumed to be under the external exciting incident plane wave. Following the MOM procedure, applying the thin wire approximation, and considering each wire element as an N subdivided segments yields an $N\times P\times Q$) linear equation set as follows [16, 23]: (see (1))

The vectors $[\boldsymbol{I}^p]=[I_{p,1}, I_{p,2},\ldots,I_{p,N}]^{\mathrm{T}}$ and $[\boldsymbol{V}^p]=[V_{p,1}, V_{p,2},\ldots,V_{p,N}]^{\mathrm{T}}$, $p=1, 2, \ldots, P$, contain samples of current and voltage distribution on the pth fed wire element, respectively. In (1), the matrix block $[\boldsymbol{Z}^{p,i}]$ can be written as follows

$$[\boldsymbol{Z}^{p,i}]=\begin{bmatrix} Z_{1,1}^{p,i} & Z_{1,2}^{p,i} & \cdots & Z_{1,N}^{p,i} \\ Z_{21}^{p,i} & Z_{2,2}^{p,i} & \cdots & Z_{2,N}^{p,i} \\ \vdots & \vdots & \ddots & \vdots \\ Z_{N,1}^{p,i} & Z_{N,2}^{p,i} & \cdots & Z_{N,N}^{p,i} \end{bmatrix} \tag{2}$$

where $Z_{j,m}^{p,i}$, $i=1,2,\ldots,(P\ Q)$, $m, j=1, 2, \ldots, N$, denotes the impedance between the mth segment of the pth fed wire element and the jth segment of ith wire element. The pth

$$\begin{bmatrix} [Z^{11}]_{N\times N} & [Z^{12}]_{N\times N} & \cdots & [Z^{1(PQ)}]_{N\times N} \\ [Z^{21}]_{N\times N} & [Z^{22}]_{N\times N} & \cdots & [Z^{2(PQ)}]_{N\times N} \\ \vdots & \vdots & \ddots & \vdots \\ [Z^{(PQ)1}]_{N\times N} & [Z^{(PQ)2}]_{N\times N} & \cdots & [Z^{(PQ)(PQ)}]_{N\times N} \end{bmatrix}_{(PQ)\times N\times(PQ)\times N} \begin{bmatrix} [I^1] \\ [I^2] \\ \vdots \\ [I^{(PQ)}] \end{bmatrix}_{((PQ)\times N)\times 1} = \begin{bmatrix} [V^1] \\ [V^2] \\ \vdots \\ [V^{(PQ)}] \end{bmatrix}_{((PQ)\times N)\times 1} \tag{1}$$

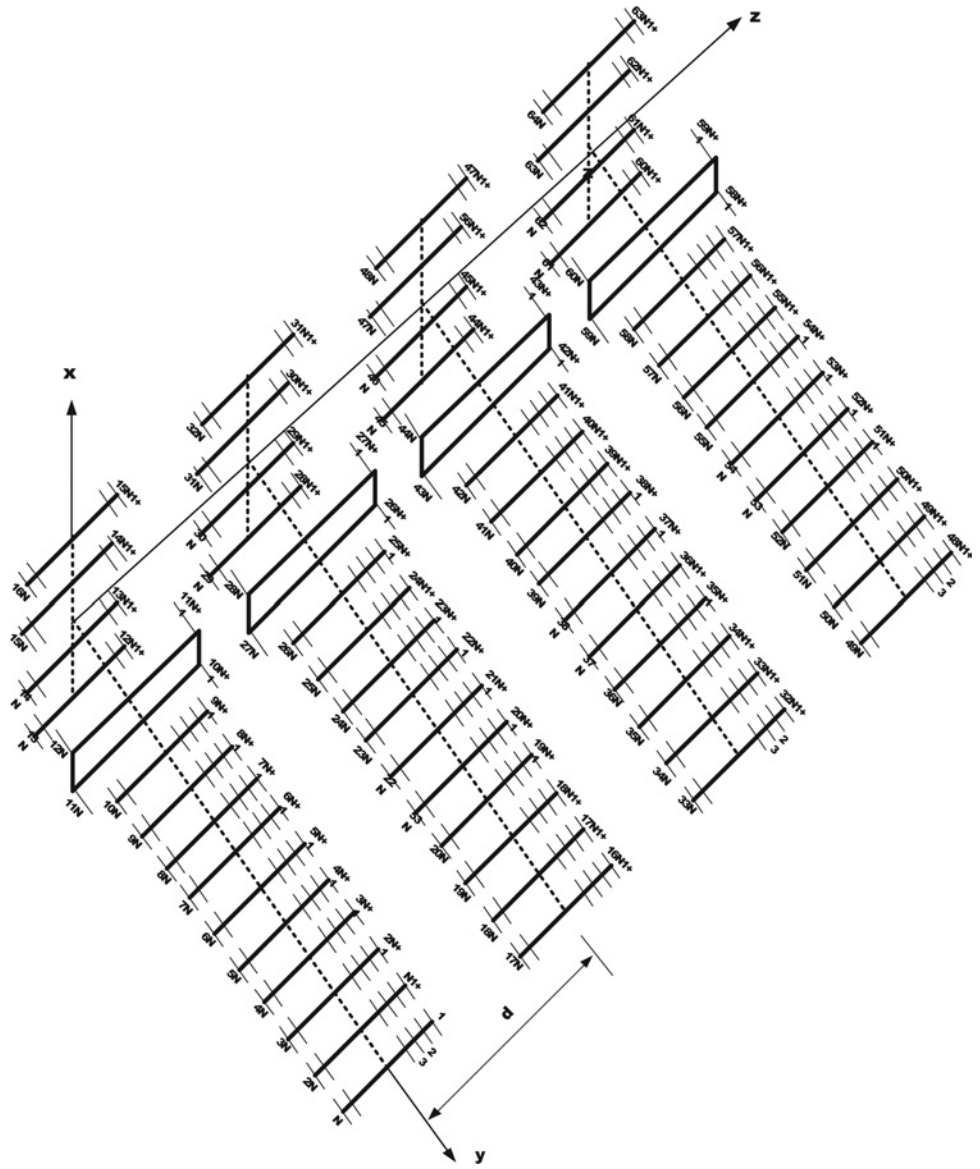

Fig. 1 *Four-element collinear VHF/UHF Yagi-Uda antenna array*

row of the matrix of (1) can be written as follows

$$[V^p] = [Z^{p,1}][I^1] + [Z^{p,2}][I^2] + \ldots + [Z^{p,p}][I^p] + \ldots + [Z^{p,(PQ)}][I^{(PQ)}] \quad (3)$$

or

$$[V^p] = [U^p] + [W^p] = [Z^{p,p}][I^p] + \{[Z^{p,1}][I^1] + \ldots + [Z^{p,p-1}][I^{p-1}] + [Z^{p,p+1}][I^{p+1}] + \ldots + [Z^{p,(PQ)}][I^{(PQ)}]\} \quad (4)$$

where $[U^P]$ is the exact system of equations resulted from the MOM analysis for the pth fed wire element if it was standing alone without the presence of all the other wire elements, and defines the voltage because of the incident plane wave on the pth fed wire element. $[U^P]$ is the desired voltage and should be found and $[W^p]$ is the voltage created by current distribution on other wire elements, which is undesired and should be eliminated. If the current distributions on all the wire elements in the Yagi-Uda antenna array are exactly known, the mutual coupling effect on the pth fed wire element could be perfectly removed. In the real situation, only the currents and voltages on the Yagi-Uda antenna terminals can be measured. To overcome the problem, one should make 'single-mode' approximation [16]. By using the currents and voltages on the Yagi-Uda antenna terminals, the Yagi-Uda antenna array as an $(P+1)$-terminal linear time invariant (LTI) network can be described. Thus, (4) will be formulated as follows [20, 21]

$$V_p = U_p + W_p = U_p + \sum_{k=1}^{P} I_k Z_t^{p,k} \quad p = 1, 2, \ldots, P \quad (5)$$

In (5), $Z_t^{p,k}$ and $Z_t^{p,p}$ specify receiving mutual and self-impedance terms between the Yagi-Uda antennas, respectively. U_P is the voltage of a Yagi-Uda antenna terminal, caused only by incident wave on the antenna and W_p is the voltage made by mutual coupling from all other antennas. $I_P = V_P/Z_L$ indicates the induced current at the terminals of the Yagi-Uda antenna. As pointed out in [20, 21], the effect of induced current on the pth Yagi-Uda antenna because of scattered fields from other Yagi-Uda

doi: 10.1049/iet-map.2013.0218

antennas are formulated by adding $Z_t^{p,p}$ term as self-impedance into the mutual coupling equations. Hence, the new MIM contains some self-impedance terms. In applications with finite Yagi-Uda antenna arrays, self-impedances $Z_t^{p,p}$ are not certainly equal for $p = 1,2,\ldots, P$. The reason is that the relative position of pth Yagi-Uda antenna, with respect to the other Yagi-Uda antennas, can alter the value of self-impedance. Rearranging (5) and writing in matrix notation, one can obtain

$$[\boldsymbol{W}] = [\boldsymbol{V}] - [\boldsymbol{U}] = [\boldsymbol{Z}_t][\boldsymbol{I}] \tag{6}$$

where $[\boldsymbol{Z}_t]$ is the $P \times P$ MIM between Yagi-Uda antennas, and $[\boldsymbol{V}] = [V_1, V_2,\ldots,V_P]^{\mathrm{T}}$ and $[\boldsymbol{U}] = [U_1, U_2,\ldots,U_P]^{\mathrm{T}}$ are the vectors containing the measured and decoupled voltages at the Yagi-Uda antenna terminals, respectively. The vector $[\boldsymbol{I}] = [I_1, I_2,\ldots,I_P]^{\mathrm{T}}$ is the induced current at Yagi-Uda antenna terminals. The MIM relates the Yagi-Uda antenna terminal currents to the coupled voltages $[\boldsymbol{W}]$, when all Yagi-Uda antennas are connected to the same load, $Z_{\mathrm{L}}^p = Z_{\mathrm{L}}$, $p = 1, 2, \ldots, P$. As mentioned earlier, when antenna elements have an omnidirectional radiation pattern, such as dipole or monopole antennas, the mutual impedances are independent of the DOA of signal. This is due to the fact that the impinging signal induces current distributions on all wire elements and the mutual impedance between antennas also accounts for the re-radiation from these current distributions. When the azimuth angle of arrival is not too far from the plane and is perpendicular to the axis of the antenna (i.e.$70° \le \varphi \le 110°$) and wire elements in Yagi-Uda antenna array have omnidirectional radiation pattern in the azimuth plane, then the induced current distribution on the all wire elements in a Yagi-Uda antenna array will be fixed with the azimuth angle of the impinging signal [13–15]. Therefore mutual impedances between antennas are invariant with respect to this range of azimuth angles. Taking advantage of this observation, the voltages and currents of Yagi-Uda antenna terminals at P distinct angles of arrival, ϕ_p, $p = 1,2,\ldots,P$, are measured. The data is then used to compute the mutual impedance between each pair of Yagi-Uda antennas. As practiced in this paper, one may assume that there is P^2 unknown elements in the MIM, and find the unknowns by formulating P^2 equations, associated with P plane wave incidence scenarios. The voltages and currents of the antenna terminals are measured for P incidence angles ϕ_p, $p = 1,2,\ldots,P$, then, (6) for this set of experiments may be written as follows [20]: (see (7))

where $\otimes$ is the Kronecker tensor product. The quantities $V_p^{\phi_p}$, $U_p^{\phi_p}$ and $I_p^{\phi_p}$, $p = 1, 2, \ldots, P$, represent the terminal voltages and currents of the Yagi-Uda antennas. These voltages and currents may be measured practically by a number of plane wave incidence scenarios or, calculated via the electromagnetic MOM algorithm for P plane wave incidence scenarios. The P^2 unknown mutual and self-impedance terms, $Z_t^{p,k}$, $p, k = 1,2,\ldots,P$, are obtained by solving (7) [20].

As we will see in Section 4, the formulation of this work, excellently, removes the mutual coupling effects and makes an absolutely essential improvement in the performance of the DOA estimation algorithms. When the spacing between the Yagi-Uda antennas of the array is reduced, the inclusion of the self-impedance terms, $Z_m^{p,p}$ to the MIM becomes increasingly vital. This is due to the fact that the coupling between the Yagi-Uda antennas of the array obtains stronger.

Fig. 2 *VHF/UHF Yagi-Uda antenna array*

$$\begin{bmatrix} V_1^{\phi_1} - U_1^{\phi_1} \\ V_1^{\phi_2} - U_1^{\phi 2} \\ \vdots \\ V_1^{\phi_{P-1}} - U_1^{\phi_{P-1}} \\ V_1^{\phi_P} - U_1^{\phi_P} \\ \vdots \\ V_P^{\phi_1} - U_P^{\phi_1} \\ V_P^{\phi_2} - U_P^{\phi_2} \\ \vdots \\ V_P^{\phi_{P-1}} - U_P^{\phi_{P-1}} \\ V_P^{\phi_P} - U_P^{\phi_P} \end{bmatrix}_{P^2 \times 1} = \left(I_{P \times P} \otimes \begin{bmatrix} I_1^{\phi_1} I_2^{\phi_1} & \cdots & I_{P-1}^{\phi_1} I_P^{\phi_1} \\ I_1^{\phi_2} I_2^{\phi_2} & \cdots & I_{P-1}^{\phi_2} I_P^{\phi_2} \\ \vdots \ \vdots & \ddots & \vdots \ \vdots \\ I_1^{\phi_{P-1}} I_2^{\phi_{P-1}} & \cdots & I_{N-1}^{\phi_{P-1}} I_N^{\phi_{P-1}} \\ I_1^{\phi_P} I_2^{\phi_P} & \cdots & I_{P-1}^{\phi_P} I_P^{\phi_P} \end{bmatrix} \right)_{P^2 \times P^2} \begin{bmatrix} Z_t^{1,1} \\ Z_t^{1,2} \\ \vdots \\ Z_t^{1,P-1} \\ Z_t^{1,P} \\ \vdots \\ Z_t^{P,1} \\ Z_t^{P,2} \\ \vdots \\ Z_t^{P,P-1} \\ Z_t^{P,P} \end{bmatrix}_{P^2 \times 1} \tag{7}$$

Fig. 3 *Transmitting antenna*

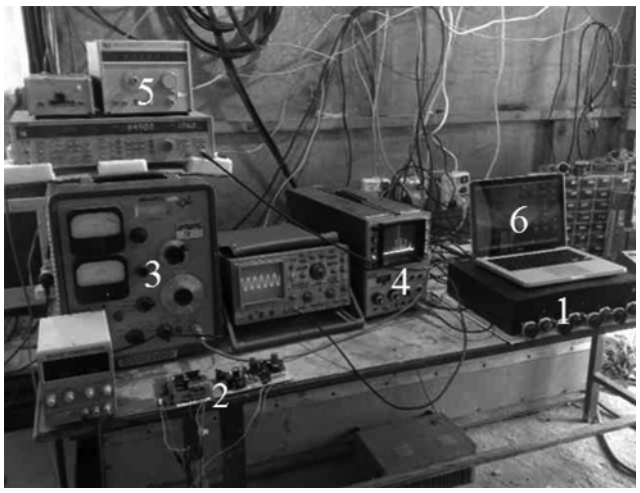

Fig. 4 *Receiver equipment*

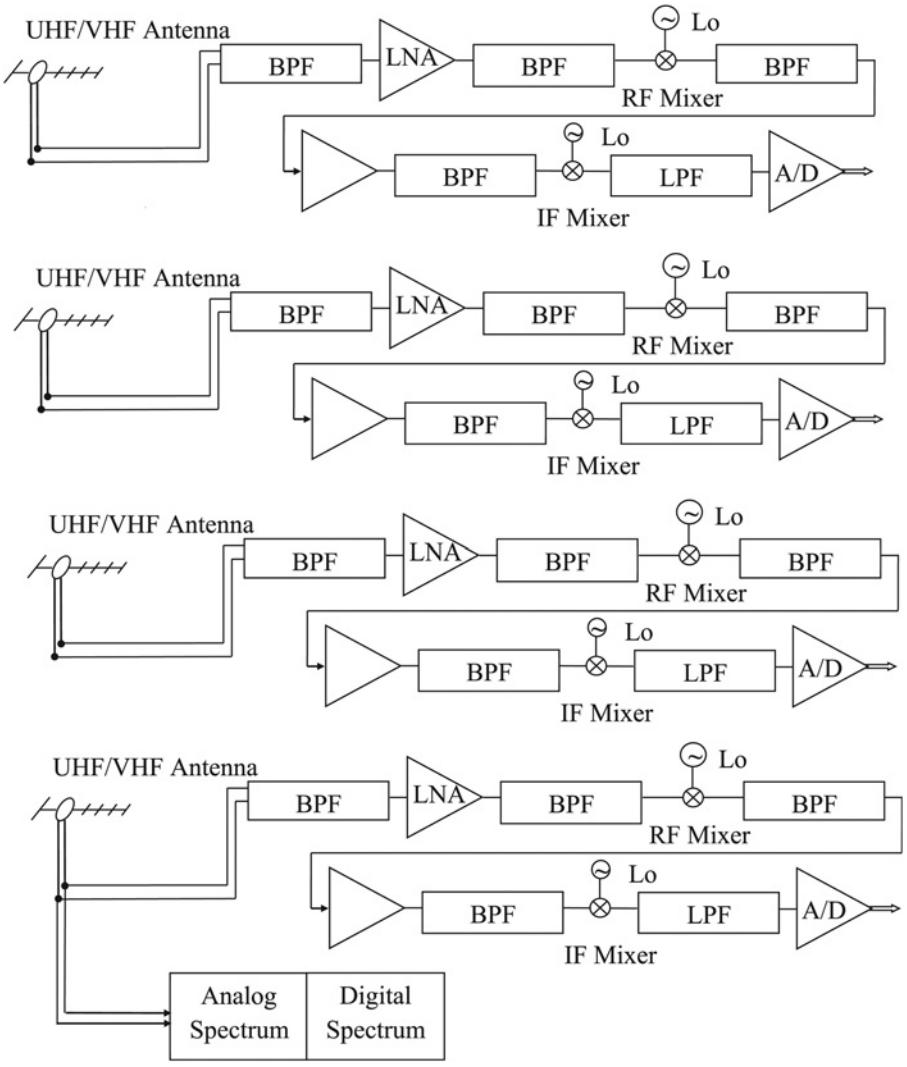

Fig. 5 *General block diagram of the receiver*

IET Microw. Antennas Propag., 2013, Vol. 7, Iss. 13, pp. 1072–1083
doi: 10.1049/iet-map.2013.0218

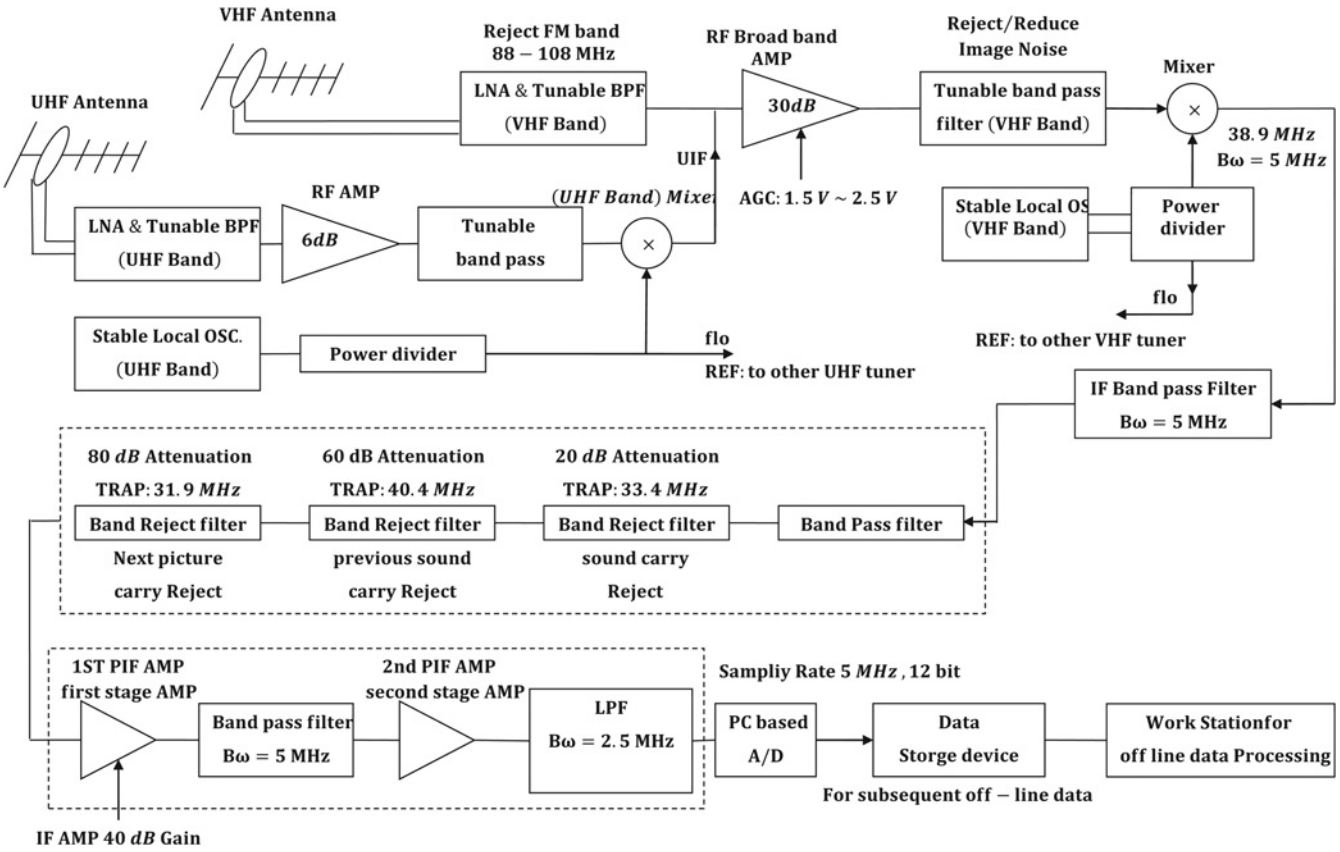

Fig. 6 *Block diagram of a single receiver channel*

3 System overview

This section is devoted to the equipment used to provide the data for this paper. The experimental data was captured using receiver equipment at the AARL-SU. The system contains four identical channels, that were used to down-convert the received signals from their transmitted frequency (i.e. 180–800 MHz) to baseband, where they were sampled, digitised and stored on a standard PC for future processes. Each channel was fed with a standard VHF/UHF Yagi-Uda antenna. The VHF/UHF Yagi-Uda antenna array is mounted on a height-adjustable antenna mast as shown in Fig. 2. The set of the VHF/UHF Yagi-Uda antenna array and antenna mast is controlled by a servo mechanism, constructed of a spiral gearbox, DC motor and a controller system with 0.1° of accuracy. The controller is designed with AVR-ATMEGA64 processor and is connectable to the computer via RS_232 connector (labelled 2 in Fig. 4). A transmitting antenna and a VHF/UHF Hewlett-Packard oscillator are utilised as in Fig. 3 to transmit plane wave with arbitrary azimuth angle with respect to the axis of the Ygai-Uda antenna array.

The receiver equipment is shown in Fig. 4. As it is delineated in Fig. 6, in each channel the signal passes through a low noise broadband amplifier which is placed on the antenna mast. In the receiver, the signal is first passed through a tunable bandpass filter then it is passed through a low noise amplifier with 30 dB of gain. A bandpass tunable filter is used to reject image noise, before being mixed down to a first IF at 38.9 MHz. The local oscillator signal was provided by an extremely stable Rohde and Schwartz (labelled 3 in Fig. 4) which also provided a reference signal that was used to phase lock the other entire block in the receiver system.

The first IF signal for further down conversion was fed into a three-stage band-reject filter to reject image noise, before being mixed down to a second IF centred at 2.5 MHz. The output of the second mixer is passed through a low-pass filter with 2.5 MHz cut-off frequency. It is then fed into an analog-to-digital convertor (ADC) in the data acquisition (DAQ) board. The acquisition board contains four ADC convertor channel with 20 MHz sampling rate and 12 bits accuracy. The data of these channels can be stored by a PC for future processes. The spectrum of the arrival signal in each channel can be viewed by using Hewlett-Packard spectrum analyser (labelled 4 in Fig. 4). General block diagram for the receiver is shown in Fig. 5.

The DAQ system consists of a PC with installed DAQ card with four analog input (AI) channels, and a graphic user interface (GUI) software. As it is known the data captured from the antenna array in the receiving mode are contaminated by undesired interferences such as noise and clutter, and so on. The GUI that is designed and introduced in this work is appropriate software for extracting desired signal from undesired interferences. Fig. 7 shows a general view of the prepared GUI. This GUI is written by MATLAB based on the available general DAQ and the accompanying ADLINK-MATLAB-toolboxes. The received signals are first sampled using installed DAQ by ADLINK Technology Inc. The spectrum of the received signals is estimated by applying a fast Fourier transform (FFT) algorithm on the sampled data. The resulting spectrum is observed in the GUI thereafter including some discernible peaks. The desired signal can be captured within a bandwidth around the frequency where the desired signal peaks are expected to exist. Finally, the data captured by above-mentioned procedure are stored to be used in the

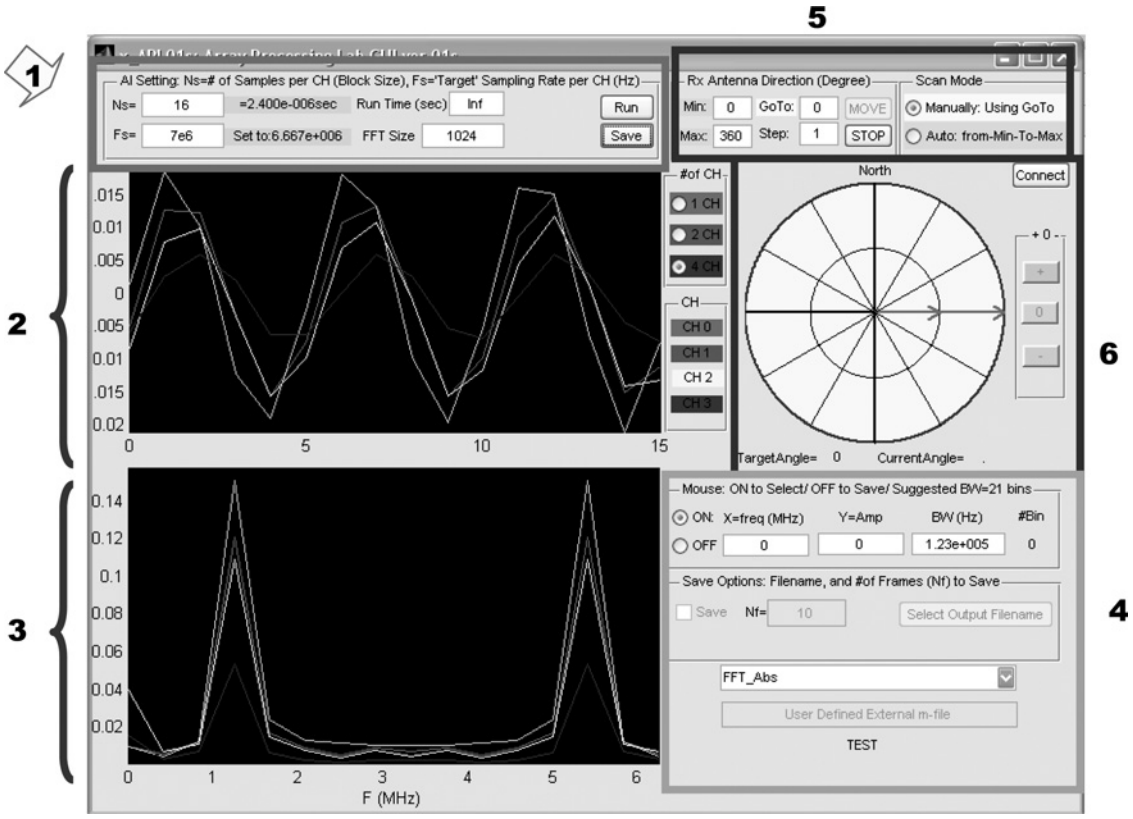

Fig. 7 *General view of the GUI*

future off-line processing. In practice, it is not necessary to store many frames of the captured data by DAQ card for off-line processing. The user is interested in specific frequency range over a centre point depending on the frequencies of the desired signals. Hence, the program should be run (for a few seconds) to observe the absolute value of the FFT to find the desirable range. The frequency in which a desired peak or centre point exists can be selected by enabling mouse ON button and then clicking on the black area of the output frame. The mouse OFF button sets the defined settings. Finally, the save options demands the number of frames required for processing. The saved file includes a structure which consists of sampling frequency (F_s), centre frequency (F_c), bandwidth around the centre frequency (BW), and a cell-array (W) which in turn, includes the number of frames of the complex FFT values. The absolute value of a typical saved frame of the desired signal is illustrated in Fig. 8*a* as an example. As shown in Fig. 8*a*, the desired signal is extracted and redundancies are omitted. Fig. 8*b* reveals the phase difference between all four channels with respect to channel zero for all the (400) saved frames.

The GUI contains different parts labelled in Fig. 7, AI settings (label 1), input data (label 2), output data (label 3),

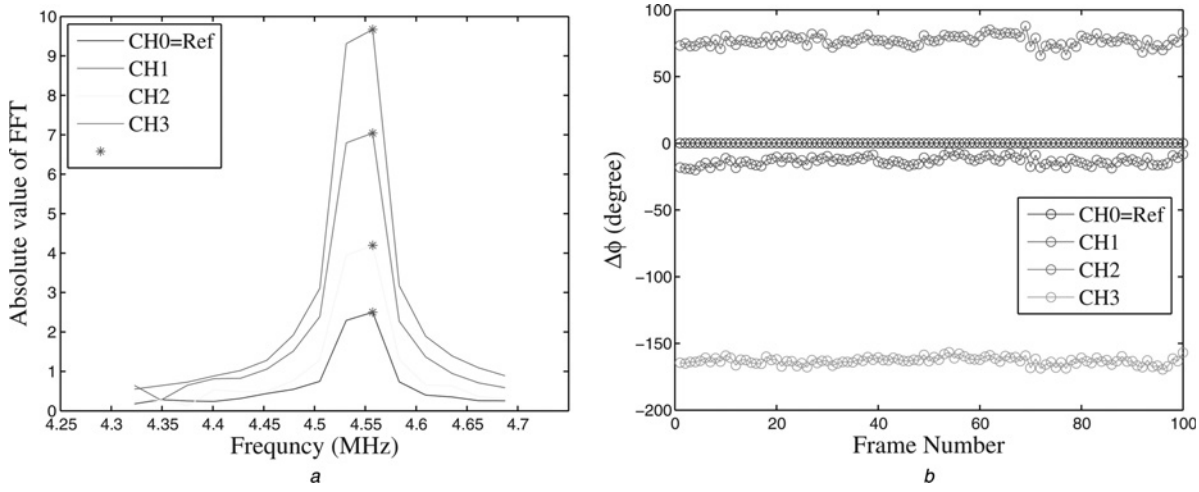

Fig. 8 *Results of typical off-line processing on the saved frames*

a Absolute value of the FFT of desired signal
b Phase differences among the channels with respect to the channel zero for all 400 frames

doi: 10.1049/iet-map.2013.0218

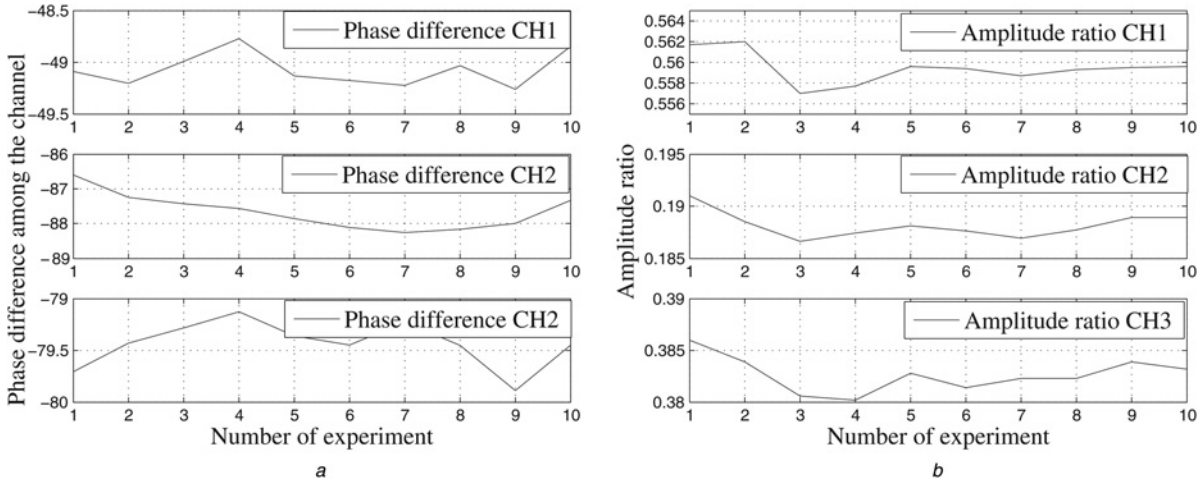

Fig. 9 *System accuracy*

a In measuring phase differences
b In measuring amplitudes ratio

data processing (label 4), antenna's rotation control system settings (label 5) and antenna's direction display (label 6). In order to apply the FFT algorithm, antenna output should be sampled in an A/D convertor in which the number of samples (NS) should be allocated per channel. The simultaneous sampling frequency of all channels is determined by the frequency of sampling (FS) option, which could be set to the nearest available sampling frequency by the DAQ card when the program is run. The NS and FS are shown at the top left of Fig. 7. The run time option allows the program to run the DAQ and manipulation algorithms for user's desirable duration. DAQ systems are greatly employed in passive radars, sonar systems and related subsystems such as array processing, DOA estimation, beamforming and adaptive nulling. The main role of the DAQ system is digitising the signals which impinge the sensor array and reshaping the raw data into comprehensible structure for applying required data processing algorithms. The installed DAQ card is NuDAQ PCI-9812 which is a 20 MHz simultaneous four-channel AI card with 12-bit data resolution by ADLINK Technology Inc.

In the following, the accuracy of the system is evaluated in measuring phase difference and amplitude ratio among the channels with respect to channel zero. This is carried out by testing the system and capturing experimental data from receiving equipment. In order to measure the system accuracy, a plane wave is radiated ten times to the VHF/UHF antenna array from a particular direction. All experiments are accomplished under the same conditions. Phase difference and amplitude ratio among the channels with respect to channel zero are indicated in Fig. 9.

Experimental results reveal that the MSE in measuring phase difference between channel one and channel zero is 0.0267 degree square (DS), between channel two and channel zero is 0.2735 DS and between channel three and channel zero is 0.0497 DS. Moreover, MSE of measuring the amplitude ratio of channel one to channel zero is 0.006, channel two to channel zero is 0.0034 and channel three to channel zero is 0.0015.

Table 1 Signal parameters for DOA estimation

	First signal	Second signal
frequency	470 MHz	470 MHz
polarisation	horizontal	horizontal
SNR	3 dB	3 dB
arrival angle	$\varphi = 75°$	$\varphi = 105°$

4 Experimental and simulation results

In this section, the mutual coupling compensation capability of the proposed method for a practical four-element VHF/UHF Yagi-Uda antenna array is evaluated experimentally. For the evaluation of the mutual coupling compensation capability of the proposed scheme, three scenarios are performed. In the first experiment, two signals impinge the array from horizontal direction ($\theta = 90°$) and azimuth angles $\varphi = 75°$ and 105°. In this case the Yagi-Uda antenna terminals are connected to the 300 Ω load whereas the distance between Yagi-Uda antennas is $d = 0.5\lambda$. To demonstrate the statistical performance of the proposed method, the Monte Carlo experiments, that is 100 trials for

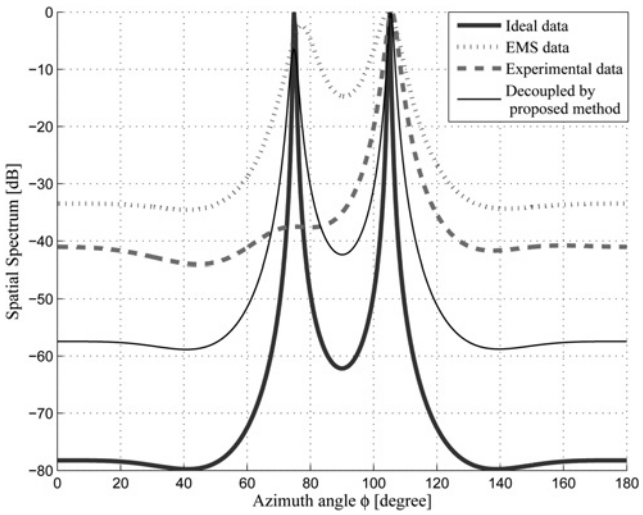

Fig. 10 *Spatial spectrum of the MUSIC algorithm for the detection of the two incoherent signals of Table 1, with P = 4, d = 0.5λ, a = λ/200 and Z_L = 300 Ω*

Table 2 Detection results

Input data/direction	Algorithms	$\theta_1 = 90°, \varphi_1 = 75°$		$\theta_2 = 90°, \varphi_2 = 105°$	
		$E[\hat{\varphi}_1]$	$\lvert\varphi_1 - E[\hat{\varphi}_1]\rvert$	$E[\hat{\varphi}_2]$	$\lvert\varphi_2 - E[\hat{\varphi}_2]\rvert$
ideal data (without mutual coupling)	MUSIC	74.80°	0.20°	105.10°	0.10°
	root-MUSIC	74.98°	0.02°	105.02°	0.02°
	ESPRIT	74.98°	0.02°	105.02°	0.02°
EMS data (with mutual coupling)	MUSIC	77.20°	2.20°	104.7°	0.30°
	root-MUSIC	76.70°	1.70°	104.94°	0.06°
	ESPRIT	77.09°	2.09°	104.94°	0.06°
experimental data (with mutual coupling)	MUSIC	fail	fail	105.6°	0.40°
	root-MUSIC	fail	fail	105.77°	0.77°
	ESPRIT	fail	fail	105.29°	0.29°
experimental data (compensate by proposed method)	MUSIC	74.80°	0.20°	105.3°	0.30°
	root-MUSIC	74.42°	0.58°	105.26°	0.26°
	ESPRIT	74.78°	0.22°	105.38°	0.38°

each simulation is performed. In addition, the arrival signals are contaminated with an additive white Gaussian noise (AWGN) with a signal-to-noise ratio (SNR) of 3 dB. In each trial 256 snapshots of data were captured and processed by the high-resolution DOA estimation algorithms. To evaluate the performance of high-resolution DOA estimation algorithms for a practical VHF/UHF Yagi-Uda antenna array, four different types of voltages are applied as input to these algorithms. Root mean square error (RMSE) of advanced subspace-based algorithms such as MUSIC, root-MUSIC and ESPRIT are obtained and compared with each other, using four types of input data. The first type is the ideal terminal voltages without mutual coupling effect. The second type is the terminal voltages obtained by the full-wave electromagnetic MOM algorithm (EMS data). The third type is practical terminal voltages captured from the VHF/UHF Yagi-Uda antenna array based at the AARL-SU. Finally, the fourth type is practical terminal voltages modified by the proposed method of this work. The spatial spectrum of MUSIC algorithm and the results summary of DOA estimation by MUSIC, root-MUSIC and ESPRIT algorithms for detecting two incoherent signals that are described in Table 1 are illustrated in Fig. 10 and tabulated in Table 2, respectively.

As shown in Fig. 10 and Table 2, using the ideal terminal voltages without mutual coupling effect, three algorithms detect the two incoherent signals, with an accuracy of $\pm 0.2°$. By applying the EMS terminal voltages, the two signals are detected, however, the peak of the signals are not sharp enough and there are a displacement of $\pm 2.2°$. Using the practical terminal voltages, all algorithms detect only one peak at $\varphi = 105°$, with an accuracy of $\pm 0.77°$ whereas the signal is completely missed at $\varphi = 75°$. This is due to the mutual coupling effect between Yagi-Uda antennas. As clearly observed from Fig. 10 and Table 2, if the practical terminal voltages are compensated by using the proposed method, there will be sharper peaks for both angles of arrivals, $\varphi = 75°$ and 105° with detection biases less than $\pm 0.38°$ for all cases.

To compute the RMSE of DOA estimation for each snapshot or SNR, we used the results of 100 experiments. In this case a signal comes from horizontal direction ($\theta = 90°$) and azimuth angle $\varphi = 105°$. RMSE of the MUSIC, root-MUSIC and ESPRIT algorithms are plotted for four types of input data against the number of snapshots and SNR variations in Figs. 11*a–f*. As Fig. 11 shows, the RMSE curves of experimental and EMS data are higher than other kinds of data, even for high SNR. In addition, RMSE curves of experimental and EMS data reveal that RMSE has a particular lower bound and cannot be less than a lower bounds as the number of snapshots and SNR (i.e. more than 50 snapshots and SNR = -3 dB) increases. The reason is that experimental and EMS data are affected by mutual coupling effects between the antennas.

These figures, clearly, show that if practical terminal voltages are decoupled using the proposed method, nearly perfect decoupling of terminal voltages is achieved. It can be deduced that the application of a MUSIC, root-MUSIC and ESPRIT algorithms to the decoupled terminal voltages leads to an excellent performance of DOA estimation in terms of accuracy and resolution, even for low SNR. As shown in Fig. 11 and Table 2, the bias is small in comparison to the RMSE in each case.

In the second experiment, the performance of MUSIC, root-MUSIC and ESPRIT algorithms are compared through the Monte Carlo experiments for each type of data. Therefore a signal comes from the vertical angle $\theta = 90°$ and azimuth angle $\varphi = 105°$. RMSE of the three algorithms are plotted against SNR for each ideal data, EMS data, experimental data and decoupled experimental data as in Figs. 12*a–d*. In each case, 100 trials for each SNR were performed, and in each trial 256 data snapshots were captured and processed by the high-resolution DOA estimation algorithms. The results are illustrated in Figs. 12*a–d*.

It can be inferred from Fig. 12*a* that in ideal situations, RMSE of the DOA estimation methods decreases as SNR increases. It is also revealed that root-MUSIC shows better performance than the other two algorithms. On the contrary, in practical situations ESPRIT algorithm shows better performance than the other two algorithms as one can see from Figs. 12*c* and *d*.

As the last experiment, the performance of ESPRIT algorithm for two signals that are coming from elevation angles $\theta_1 = \theta_2 = 90°$ and azimuth angles $\varphi_1 = 105°$, $\varphi_2 = 120°$ are compared through the Monte Carlo experiments. In order to capture experimental data, the output of VHF/UHF Yagi-Uda antenna array is gathered two times, each time a signal impinge the array from specific angle of arrival. To compute the estimated RMSE for each SNR the results of the 100 experiments have been used. In each experiment 256 snapshots of practical data were captured from VHF/UHF Yagi-Uda antenna array. At first, the captured data was modified by the proposed method of this work and then processed by the ESPRIT algorithms. The results are shown in Fig. 13.

doi: 10.1049/iet-map.2013.0218

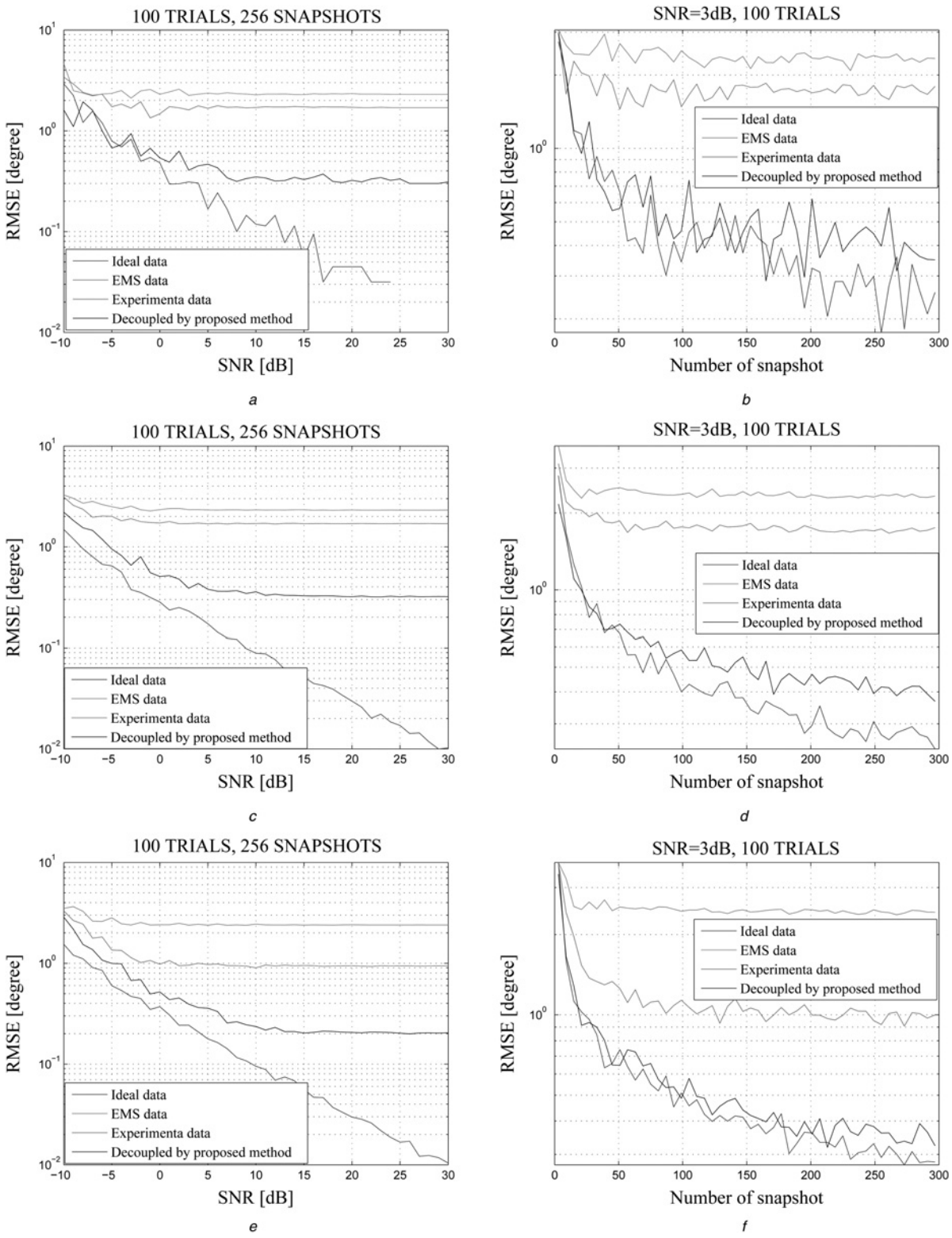

Fig. 11 *RMSE of the MUSIC, root-MUSIC and ESPRIT algorithms for different types of voltages as input of these algorithms against SNR and number of snapshots*

a MUSIC algorithm against SNR
b MUSIC algorithm against number of snapshots
c Root-MUSIC algorithm against SNR
d Root-MUSIC algorithm against number of snapshots
e ESPRIT algorithm against SNR
f ESPRIT algorithm against number of snapshots

As delineated in Fig. 13, RMSE of the DOA estimation is the functions of signal's DOA. In other words, RMSE increases as the angle of arrival of incoming signal recedes from the line of sight (LOS). Based on the experimental and simulation results it is concluded that mutual coupling effect between array elements is the functions of signal's DOA.

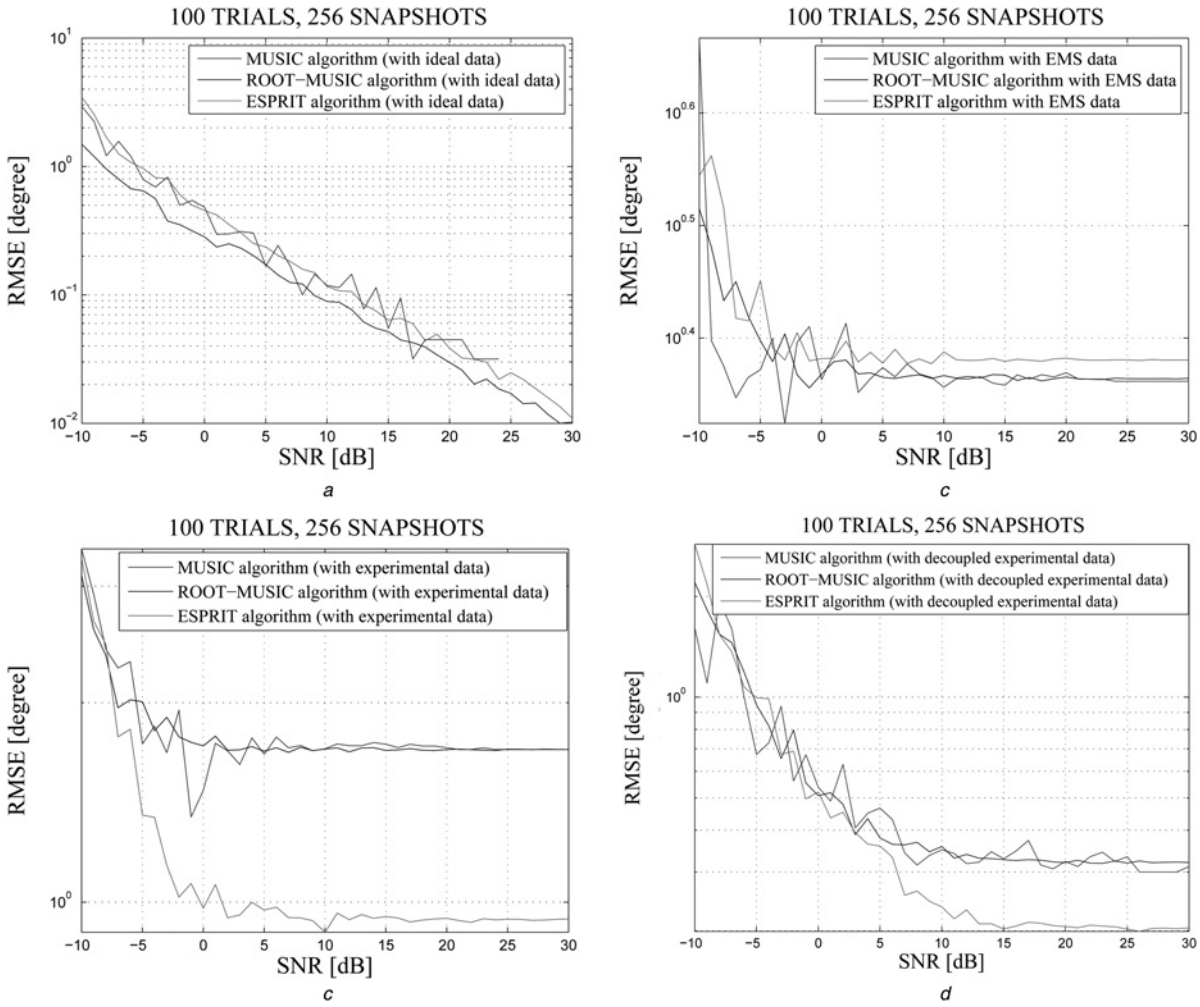

Fig. 12 *RMSE of the MUSIC, root-MUSIC and ESPRIT algorithms against SNR*

a Ideal data
b EMS data
c Experimental data
d Decoupled experimental data

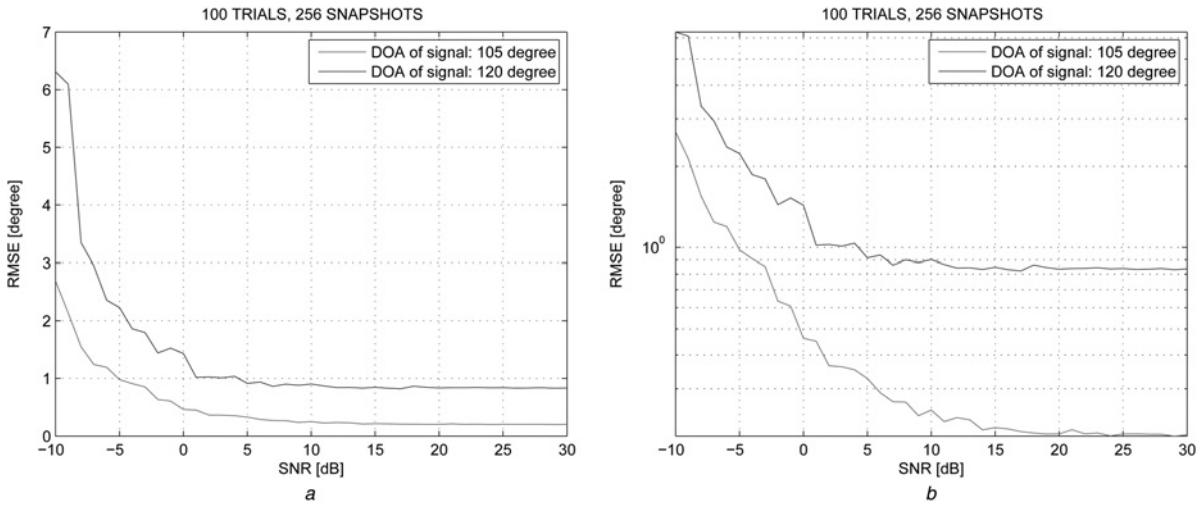

Fig. 13 *RMSE of ESPRIT algorithm for modified experimental data against SNR*

5 Conclusion

In this paper, for the first time, a decoupling methodology for compensating mutual coupling effect in a practical VHF/UHF Yagi-Uda antenna array is introduced by using a new MIM model. In the proposed scheme, extreme care has been taken into account for both self-impedance and mutual impedance, related to the mutual coupling effects. The

doi: 10.1049/iet-map.2013.0218

MIM is calculated through a number of measured voltages and currents of Yagi-Uda antenna terminals. These voltages and currents were captured by a number of plane wave incidence scenarios. Using the proposed MIM, perfect decoupling of experimental data is achieved. Experimental and simulation results demonstrated that the application of high-resolution DOA estimation algorithms to the decoupled experimental data leads to excellent performance of DOA estimation, in terms of accuracy and resolution. The performance of high-resolution DOA estimation algorithms such as MUSIC, Root-MUSIC and ESPRIT are evaluated for a practical VHF/UHF Yagi-Uda antenna array. As it is shown, regarding experimental and simulation results, in practical situations, the mutual coupling effect between array elements and RMSE of the estimated parameters are the function of signal's DOA, and in the presence of mutual coupling, ESPRIT algorithm shows better performance than other subspace-based algorithms.

6 References

1 Schmidt, R.O.: 'Multiple emitter location and signal parameter estimation', *IEEE Trans. Antennas Propag.*, 1986, **34**, (3), pp. 276–280
2 Shan, T.J., Wax, M., Kailath, T.: 'On spatial smoothing for estimation of coherent signals', *IEEE Trans. Acoustic Speech, Signal Process.*, 1985, **33**, (4), pp. 806–811
3 Roy, R., Kailath, T.: 'ESPRIT–Estimation of signal parameters via rotational invariance techniques', *IEEE Trans. Acoustics Speech Signal Process.*, 1989, **37**, (7), pp. 984–995
4 Paulraj, A., Roy, R., Kailath, T.: 'A subspace rotation approach to signal parameter estimation', *Proc. IEEE*, 1986, **74**, (7), pp. 1044–1046
5 Barabell, A.J.: 'Improving the resolution performance of eigenstructure-based direction-finding algorithms', Proc. ICASSP, Boston, 1983, vol. 8, pp. 336–339
6 Lau, C.K.E., Adve, R.S., Sarkar, T.K.: 'Minimum norm mutual coupling compensation with application in direction of arrival estimation', *IEEE Trans. Antennas Propag.*, 2004, **52**, (8), pp. 2034–2041
7 Friedlander, B., Weiss, A.: 'Direction finding in the presence of mutual coupling', *IEEE Trans. Antennas Propag.*, 1991, **39**, (3), pp. 273–284
8 Gupta, I.J., Ksienski, A.A.: 'Effect of mutual coupling on the performance of adaptive arrays', *IEEE Trans. Antennas Propag.*, 1983, **31**, (5), pp. 785–791
9 Leou, M.L., Yeh, C.C., Ucci, D.R.: 'Bearing estimations with mutual coupling present', *IEEE Trans. Antennas Propag.*, 1989, **37**, (10), pp. 1332–1335
10 Pasala, K.M., Friel, E.M.: 'Mutual coupling effects and their reduction in wideband direction of arrival estimation', *IEEE Trans. Aerosp. Electron. Syst.*, 1994, **30**, (4), pp. 1116–1122
11 Yuan, H., Hirasawa, K.: 'The mutual coupling and diffraction effects on the performance of a CMA adaptive array', *IEEE Trans. Veh. Tech.*, 1998, **47**, (3), pp. 728–736
12 Adve, R.S., Sarkar, T.k.: 'Compensation for the effects of mutual coupling on direct data domain adaptive algorithms', *IEEE Trans. Antennas Propag.*, 2000, **48**, (1), pp. 86–94
13 Hui, H.T.: 'Improved compensation for the mutual coupling effect in a dipole array for direction finding', *IEEE Trans. Antennas Propag.*, 2003, **51**, (9), pp. 2498–2503
14 Hui, H.T.: 'A new definition of mutual impedance for application in dipole receiving antenna arrays', *IEEE Antennas Wirel. Propag. Lett.*, 2004, **3**, (1), pp. 364–367
15 Hui, H.T., Low, H.P., Zhang, T.T., Lu, Y.L.: 'Receiving mutual impedance between two Normal-Mode Helical Antennas (NMHAs)', *IEEE Antennas Propag. Mag.*, 2006, **48**, (4), pp. 92–96
16 Hui, H.T.: 'A practical approach to compensate for the mutual coupling effect of an adaptive dipole array', *IEEE Trans. Antennas Propag.*, 2004, **52**, (5), pp. 1262–1269
17 Zhang, T.T., Hui, H.T., Lu, Y.L.: 'Compensation for the mutual coupling effect in the ESPRIT direction finding algorithm by using a more effective method', *IEEE Trans. Antennas Propag.*, 2005, **53**, (4), pp. 1552–1555
18 Yu, Y., Hui, H.T., Leong, M.S.: 'Receiving mutual impedance of a compact patch antenna array with two elements in a rich multipath environment'. Proc. of APMC, Asia Pacific, 2009, pp. 1751–1754
19 Lui, H.S., Hui, H.T.: 'Improved mutual coupling compensation in compact antenna arrays', *IET Microw. Antennas Propag.*, 2010, **4**, (10), pp. 1506–1516
20 Parhizgar, N., Alighanbari, A., Masnadi-Shirazi, M.A., sheikhi, A.: 'A modified decoupling scheme for receiving antenna array with application to DOA estimation', *Int. J. RF Microw. Comput. Aided Eng.*, 2013, **23**, (2), pp. 246–259
21 Parhizgar, N., Masnadi-Shirazi, M.A., Alighanbari, A., Lsur, A.: 'Adaptive nulling of a linear dipole array in the presence of mutual coupling'. Int. J. RF Microw. Comput. Aided Eng., 2013, doi:/10.1002/mmce.20709
22 Celik, N., Iskander, M.F., Emrick, R., Zhang, Z.: 'Experimental evaluation of the hybrid smart antenna system with directional array elements'. IEEE APSURSI, Antennas and Propagation Society Int. Symp., 2009, pp. 1–4
23 Gibson, W.C.: 'The method of moment in electromagnetic' (Chapman and Hall/CRC, 2008)
24 Harrington, R.F.: 'Field computation by moment methods' (IEEE Press, New York, 1993)